Desalination and Water Treatment
www.deswater.com

doi: 10.5004/dwt.2017.20601

74 (2017) 383–394
May

Adsorption of Malachite Green on Fe-modified biochar: influencing factors and process optimization

Esra Kulaksiz[a], Belgin Gözmen[b], Berkant Kayan[a], Dimitrios Kalderis[c,*]

[a]*Department of Chemistry, Arts and Science Faculty, Aksaray University, Aksaray, Turkey, emails: esra_kulaksiz@hotmail.com (E. Kulaksiz), berkantkayan@aksaray.edu.tr (B. Kayan)*
[b]*Department of Chemistry, Arts and Science Faculty, Mersin University, Mersin, Turkey, email: bgozmen@yahoo.com*
[c]*Department of Environmental and Natural Resources Engineering, School of Applied Sciences, Technological and Educational Institute of Crete, Chania, Crete, Greece, Tel. +302821023017; Fax: +302821023003; email: dkalderis@chania.teicrete.gr*

Received 25 October 2016; Accepted 16 February 2017

ABSTRACT

Paper sludge and wheat husk biochar was converted to a Fe-composite through a simple co-precipitation process and its adsorption behavior was tested against an emerging pollutant, Malachite Green (MG). Response surface methodology was employed to determine the optimum experimental conditions and the interactions between pH, initial MG concentration, temperature and treatment time. The maximum adsorption percentage obtained experimentally was 97.1%, whereas the Box–Behnken design predicted a maximum adsorption of 98%, at pH 6.16, initial MG concentration of 6.56 ppm, temperature of 34.75°C and treatment time of 22 min. Compared with the original biochar, the Fe-modified sample improved the adsorption of MG by ~34%. The adsorption mechanism followed the Langmuir model (q_{max} = 172.3 mg/g, correlation coefficient 0.960) and the kinetics of the process were best described by the pseudo-second-order model (correlation coefficient 0.9818), although boundary layer effects were also observed.

Keywords: Biochar; Malachite Green; Adsorption; Fe-modified composite; Response surface methodology

1. Introduction

Malachite Green (MG) is a water-soluble, synthetic basic dye used in the processing of different materials such as silk, wool, cotton and paper (IUPAC name: [4-[[4-(dimethylamino)phenyl]-phenylmethylidene]cyclohexa-2,5-dien-1-ylidene]-dimethylazanium; chloride). Another important use of MG is in aquaculture and is considered by the fish farming industry experts as an effective antifungal and anti-protozoal drug. It has been used for the treatment of various diseases in fish and applied as a topic antiseptic. When fish is treated with MG, the substance will be absorbed and metabolized in their tissues. Both MG and one of its major lipophilic metabolites, namely leucomalachite green (LMG), pose a significant environmental threat and persist in fish tissues for a longer period of time [1,2]. The USA, EU and Canada have banned the use of MG as a veterinary drug on food of animals, aquaculture or fish for human consumption. However, due to its low cost and antiparasitic efficiency MG is still being used illegally. Concerns about the potential for human toxicity of MG and LMG have led the EU to establish a level of 2 μg/kg for MG and LMG residues in aquatic products [3].

Due to their biorecalcitrance, MG and LMG are not readily degraded using biological methods. Therefore, several physical and chemical treatment protocols have been developed to remove or degrade MG and LMG from aqueous samples. Composite nanomaterials have been in the center of these treatment methods, either as catalysts in photodegradation or as adsorbent materials. Pt/ZnO nanoparticles [4], Keggin-type polyoxometalates [5], guar gum/Al_2O_3 nanocomposites [6] and fluorine-doped ZnO

* Corresponding author.

nanowires [7] have all been successfully employed as photocatalysts to achieve >90% MG oxidation in aqueous solutions. Adsorption of MG onto various matrices has also proved an efficient treatment method. Zinc sulfide, copper oxide and magnetite nanoparticles on activated carbon support have shown promising behavior in ultrasound-assisted adsorption of MG [8–11]. Certain nanocomposite materials have also performed well in conventional adsorption experiments. Using Fe-modified cross-linked poly(methyl acrylate) at a natural pH value, Pourjavadi and Abedin-Moghanaki [12] achieved an adsorption capacity of 890 mg/g for MG. Similarly, Brigante et al. [13] coated nanosized magnetite on mesoporous silica shells and achieved an adsorption capacity of 542 mg/g. Other materials that have shown considerable potential are N-doped carbon nanotubes stabilized Cu_2O nanoparticles [14], MnO_2-modified mesoporous silica [15] and *Cerastoderma lamarcki* shells [16]. Alternative methods that have been used to degrade MG without the use of nanocomposites are electro-Fenton oxidation [17] and enzymatic biodegradation with lacasse [18].

The scope of this study was to investigate the removal of MG from aqueous solution using biochar prepared from a mixture of paper sludge and wheat husks. Biochar is the solid product of biomass pyrolysis and its uses and applications have been increasing steadily. A wide range of biomasses can be used to prepare biochar – sewage sludge, agricultural residues and fruit processing waste are just a few. The final product properties depend on pyrolysis conditions (type of furnace, heating rate, final temperature and residence time) and initial biomass properties. Most biochar works investigate its behavior as a soil amendment and its benefits on crop production [19–21]. Other research teams have focused on the adsorptive properties of biochar toward heavy metals on contaminated soil and wastewater. It has been established that engineered biochars can remove and/or immobilize heavy metals from soil and water [22–25]. Additionally, they have proven successful in removing a range of other hazardous inorganic and organic substances from wastewaters, indicating their potential to replace the more costly activated carbons in that area. For example, ammonium [26], pharmaceutically active compounds [27,28] and dyes [29–31] have been quantitatively removed from aqueous solutions.

In this paper, the biochar used was Fe-modified in order to improve its adsorption behavior and ease of recovery after treatment [32]. The composite was characterized and tested against MG adsorption from aqueous solutions. The influence of pH, contact time, temperature and initial MG concentration were examined by using a four factor Box–Behnken design combined with response surface methodology (RSM). RSM is a combination of mathematical and statistical techniques used to study the effect of several variables influencing the responses by varying them simultaneously and carrying out limited number of experiments. The validity of the method has been well established for a wide range of adsorbents and adsorption experimental designs. Finally, the adsorption mechanism and kinetics of the process were further studied by applying well-known isotherms and kinetic models.

2. Material and methods

2.1. Materials

Biochar prepared from paper sludge and wheat husks was obtained from Sonnenerde GmbH (Riedlingsdorf, Austria) and used as received. The sample was prepared through conventional pyrolysis at 500°C at a residence time of 20 min. No inert gas was used as flush gas to drive off pyrolytic vapors. The biochar was allowed to gas out for 5 min and was quenched with water to 30% water content. The detailed production conditions and full characterization of the material can be found in Bachmann et al. [33]. A brief summary of the sample properties in terms of elemental analysis (CHNS/O), heavy metals (Cd, Cr, Cu, Ni, Pb and Zn), other elements of interest (P, K, Na, Mg, Mn, Ca and Fe), pH, electrical conductivity and ash content is provided in Table 1. MG (CI 42000, molecular weight 364.91 g/mol) and all chemicals used to prepare the Fe-modified biochar were obtained from Sigma-Aldrich (Turkey). A stock solution of MG was initially prepared at a concentration of 100 ppm. Each working solution was then prepared at the required concentrations by serial dilution of the stock solution with ultrapure water. The pH was adjusted by addition of either 0.1 M HCl or 0.1 M NaOH and the pH value was monitored with a Hanna HI 2211 model digital pH-meter (USA).

2.2. Preparation and characterization of Fe-modified biochar

Fe-modified biochar was prepared through chemical precipitation of iron oxide nanoparticles on the biochar surface in a basic environment. The process is reported in detail in Kamboh and Yilmaz [34] and is briefly described below. $FeCl_2{\cdot}4H_2O$ (19.88 g), $FeCl_3{\cdot}6H_2O$ (13.32 g), HCl (5 mL–5 M), ultrapure water (40 mL) and ethanol (5 mL) were mixed in a 100 mL flask followed by gentle heating below 50°C until complete dissolution of the salts. Biochar (1 g) was then added in 30 mL of this solution and stirred for 2 h at room temperature. The suspension was then filtered, washed with water and poured into a 1 M ammonia solution. After a further 2 h of stirring, Fe-modified biochar (with Fe_3O_4 particles embedded) was collected by magnet, washed to neutral pH with distilled water, dried in vacuum at 50°C for 24 h and finally stored for further use.

Table 1
Properties of biochar used to prepare the Fe-modified composite

C (%)	51.1	Cd (mg/kg)	0.17
H (%)	1.73	Cr (mg/kg)	8.8
N (%)	1.39	Cu (mg/kg)	28.7
S (%)	0.116	Ni (mg/kg)	7.4
O (%)	12.1	Pb (mg/kg)	17.4
Ash content (%)	34.78	Zn (mg/kg)	57.4
P (mg/kg)	6,054	pH	9.30
K (mg/kg)	10,016	Conductivity (μS/cm)	1,054
Na (mg/kg)	308		
Mg (mg/kg)	3,234		
Mn (mg/kg)	127		
Ca (mg/kg)	62,219		
Fe (mg/kg)	1,550		

Fe-modified biochar (before and after MG adsorption) was morphologically characterized in a Zeiss/Supra 55 (Germany) high-resolution scanning electron microscope (SEM). The infrared (IR) spectra of Fe-modified biochar and MG-loaded Fe-modified biochar (as KBr pellets) were recorded by using an IR spectrophotometer PerkinElmer FTIR (USA) with an attenuated total reflectance attachment within the wave number in the range of 400–4,000 cm^{-1}. Energy-dispersive X-ray (EDX) spectroscopy analysis was done using a Quantax Instrument (Bruker, USA). The surface chemistry of the composite during adsorption was investigated further through the determination of the pH point of zero charge (pH_{pzc}). At pH values above the zero point charge, the surface of the adsorbent has a net negative or anionic charge, and the surface would promote cation attraction, and cation exchange reactions. At pH values below the zero point charge, the surface has a net positive charge; it will attract anions and consequently participate in anion exchange reactions. The pH_{pzc} was determined using the methodology described in Newcombe et al. [35]. The surface area and pore structure of both original and Fe-modified biochar were investigated through nitrogen adsorption at 77 K using a Micromeritics TriStar 3000.

2.3. MG adsorption method

Ultrasound-assisted adsorption was performed to study the effect of pH, treatment time, initial MG concentration and temperature on MG removal. The method followed can be seen in detail in Bagheri et al. [36] and is briefly described below. At each run, 20 mL of MG solution of known concentration and pH (as determined by the Box–Behnken design) was poured into a 50 mL Erlenmeyer flask and placed into an ultrasonic bath. Fe-modified biochar (75 mg) was added in the flask and the mixture was sonicated at a specified time and temperature (as determined by the Box–Behnken design). At the end of each run, the adsorbent was collected by a magnet and the residual MG concentration in the solution was measured in a UV–Vis spectrophotometer through absorbance at 620 nm. The removal percentage (%) and the adsorption capacity (q_e, mg/g) at equilibrium were calculated as follows:

$$\%\ \text{Removal} = \frac{C_0 - C_e}{C_0} \times 100 \tag{1}$$

$$q_e = \frac{(C_0 - C_e)V}{m} \tag{2}$$

where C_0 is the initial MG concentration (mg/L), C_e is the residual MG concentration in solution (mg/L), V is volume of MG solution (mL) used in each run and m the quantity of biochar (g).

2.4. Design of experiments

Experimental design is a specific set of experiments defined by a matrix composed by the different level combinations of the variables studied [37]. The aim is to optimize the levels of selected variables to achieve the best response. The most influential experimental variables can also be determined. The mean response is modeled as a polynomial function of the level X of the factor, and the points form the response curve. The standard model for polynomial regression includes linear and quadratic variables as well as interaction terms.

$$Y = \beta_0 + \sum_{I=1}^{k} \beta_i X_i + \sum_{I=1}^{k} \beta_{ii} X_i^2 + \sum_i \sum_j \beta_{ij} X_i X_j + \varepsilon \tag{3}$$

where β_0 is constant coefficient, β_i, β_{ii} and β_{ij} are the coefficients of the linear, quadratic and interaction effects between the i-th and j-th factors, X_i and X_j are the independent variables, k is the number of variables and ε is the residual error. The removal percentage was considered as the dependent variable or response (Y).

At least three levels per factor are needed for quadratic terms to be estimable in the second-order model, for this reason 3^k factorial or 3^{k-p} (p different from 0) fractional factorial designs might be considered. For fitting a second-order response model, the Box–Behnken design is often preferred, since the total experiment number of this design is considerably reduced compared with fractional factorial designs for a large number of variables.

In order to evaluate the influence of operating parameters on the adsorption efficiency of Fe-modified biochar, four main parameters were chosen: initial MG concentration (coded as X_{Co}), pH (X_{pH}), time (X_t) and temperature (X_T). The Box–Behnken design for four factors (variables) at three levels (–1, 0, +1) resulted in 29 experiments, according to the following equation:

$$N = 2k(k-1) + cp \tag{4}$$

where k is the number of factors and cp corresponds to the number of the central points. The conditions for each of the 29 experiments are shown in Table 2. The system limits were set as: initial MG concentration 5–10 ppm, pH between 4 and 8, time 10–30 min and temperature 20°C–40°C. The average of two experimental values was used in data analysis using Design Expert 9.

MG adsorption was determined by coefficient of determination (R^2), analysis of variance (ANOVA) and surface plots. ANOVA was performed to identify the importance of each parameter, binary interactions and quadratic terms in relation to their influence on the response. Three-dimensional (3D) surface plots were drawn while holding a variable constant in the quadratic model. The experimental and predicted values were compared with validate the model (Table 2). Finally, the optimal experimental conditions for maximum MG removal were determined.

3. Results and discussion

3.1. Characterization of original and Fe-modified biochar

The FTIR spectra of original, Fe-modified biochar and MG-loaded Fe-modified biochar are shown in Figs. 1(a)–(c). Analysis of the FTIR peaks indicates the biochar surface moieties responsible for binding the MG molecules. Comparing the three spectra, the disappearance of certain bands and

Table 2
The Box–Behnken experimental design used in adsorption of MG by Fe-modified biochar

Number of experiments	X_{Co} (mg/L)	X_{pH}	X_t (min)	X_T (°C)	Adsorption %	
					Actual	Predicted
1	10.00	6.00	30	30.0	90.25	90.25
2	7.50	6.00	20	30.0	97.16	96.38
3	7.50	8.00	30	30.0	83.50	83.66
4	7.50	6.00	20	30.0	95.80	96.38
5	7.50	6.00	10	20.0	84.80	86.06
6	10.00	6.00	20	40.0	92.17	91.65
7	7.50	6.00	10	40.0	90.96	91.18
8	7.50	6.00	30	20.0	86.20	86.91
9	5.00	6.00	30	30.0	94.84	93.87
10	10.00	6.00	20	20.0	85.89	85.63
11	5.00	8.00	20	30.0	84.30	85.55
12	10.00	8.00	20	30.0	81.01	81.26
13	5.00	6.00	20	20.0	88.63	88.61
14	7.50	6.00	30	40.0	95.44	95.11
15	7.50	6.00	20	30.0	95.98	96.38
16	5.00	6.00	10	30.0	92.13	91.48
17	5.00	6.00	20	40.0	96.20	95.92
18	7.50	8.00	20	40.0	85.74	86.04
19	7.50	4.00	20	20.0	76.62	75.93
20	7.50	6.00	20	30.0	96.14	96.38
21	10.00	6.00	10	30.0	87.01	87.86
22	10.00	4.00	20	30.0	78.80	78.48
23	7.50	8.00	10	30.0	82.85	81.88
24	7.50	4.00	20	40.0	81.26	81.87
25	7.50	6.00	20	30.0	96.81	96.38
26	5.00	4.00	20	30.0	80.76	81.43
27	7.50	4.00	30	30.0	80.38	80.81
28	7.50	4.00	10	30.0	78.52	77.82
29	7.50	8.00	20	20.0	79.67	78.67

appearance of others can be observed. This indicates the breaking of chemical bonds and the formation of new ones during the conversion of biochar to Fe-modified biochar as well as during the adsorption of MG. The main difference between Figs. 1(a) and (b) is the emerging broad peak at 3,322 cm^{-1} due to the presence of hydroxyl groups (–OH) on Fe-modified biochar. This is probably due to the use of $FeCl_3$ in the co-precipitation stage, which leads to the partial coating of the biochar surface with ferric oxyhydroxide (FeOOH) [32]. As shown in Fig. 1(c), this peak shifts to 3,241 cm^{-1}, suggesting chemical interactions between the MG molecule and the –OH group [38]. The –C=O stretching vibration is attributed to the peak at 1,625 cm^{-1} which is considerably enhanced after magnetization of biochar. The carbonyl and hydroxyl groups on the sorbent surface are responsible for the basic and anionic properties, respectively. Therefore, potentially both anionic and cationic substances can be adsorbed onto Fe-modified biochar's surface [29]. The absorbance peak at 1,031/1,050 cm^{-1} (due to the stretching of ether linkage –C–O–C–) completely disappears in the spectra

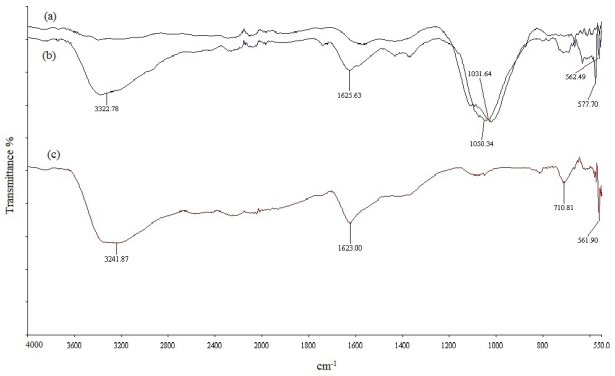

Fig. 1. FTIR spectra of: (a) original biochar, (b) Fe-modified biochar and (c) MG-loaded Fe-modified biochar.

of MG-loaded Fe-modified biochar (Fig. 1(c)). This indicates the participation of the –C–O–C– linkage in MG adsorption. Oxygen containing functional groups often play a significant role in the adsorption or binding process [39]. The bands below 800 cm^{-1} correspond to Fe–O bond deformations, therefore, confirm the formation of Fe_3O_4 particles on the biochar surface. Their absence and formation can be clearly seen between Figs. 1(a) and (b), respectively [40].

The corresponding EDX spectra of the original biochar, Fe-modified biochar and MG-loaded Fe-modified biochar (Figs. 2(a)–(c), respectively) further established the increase of Fe on the biochar surface after modification. It is interesting to note the sharp decrease in Mg, Al, Si and Ca on the Fe-modified biochar (Fig. 2(b)). Fig. 2(d) shows the relative weight of the elements during the three stages of the experimental process. It appears that magnetite was connected to the biochar surface by displacement of these ions or that these were leached from the original biochar during the co-precipitation process. Furthermore, the percentage of Fe remains practically the same after the adsorption process, indicating the stability of the composite which is always a desired advantage for wastewater treatment processes [22].

The SEM images obtained from the original biochar (Fig. 3(a)), Fe-modified biochar (Fig. 3(b)) and MG-loaded Fe-modified biochar (Figs. 3(c) and (d)) indicate that the surface morphologies of the three samples are distinctly different. The original biochar has a more heterogeneous structure than the Fe-modified sample, whereas MG-loaded Fe-modified biochar appears the most homogeneous of all and consisting of smaller particle sizes. The average particle diameter of this sample was measured at 40 nm.

The results of the surface area and pore analysis are shown in Table 3. After Fe modification, biochar surface area increased from 38 to 89 m^2/g. This is consistent with earlier works who reported that magnetite particles often have a higher surface area compared with that of the raw biomass, therefore, improving the surface area of the precursor [41–43]. However, Chen et al. [44] and Song et al. [45] observed the opposite trend with the biochar they used, the surface area of which was reduced after Fe modification. It is important to note that the surface area of Fe_3O_4 largely depends on its particle size – microscale magnetite (0.2 μm) has a surface area of ~6 m^2/g, whereas magnetite nanoparticles' (~50 nm)

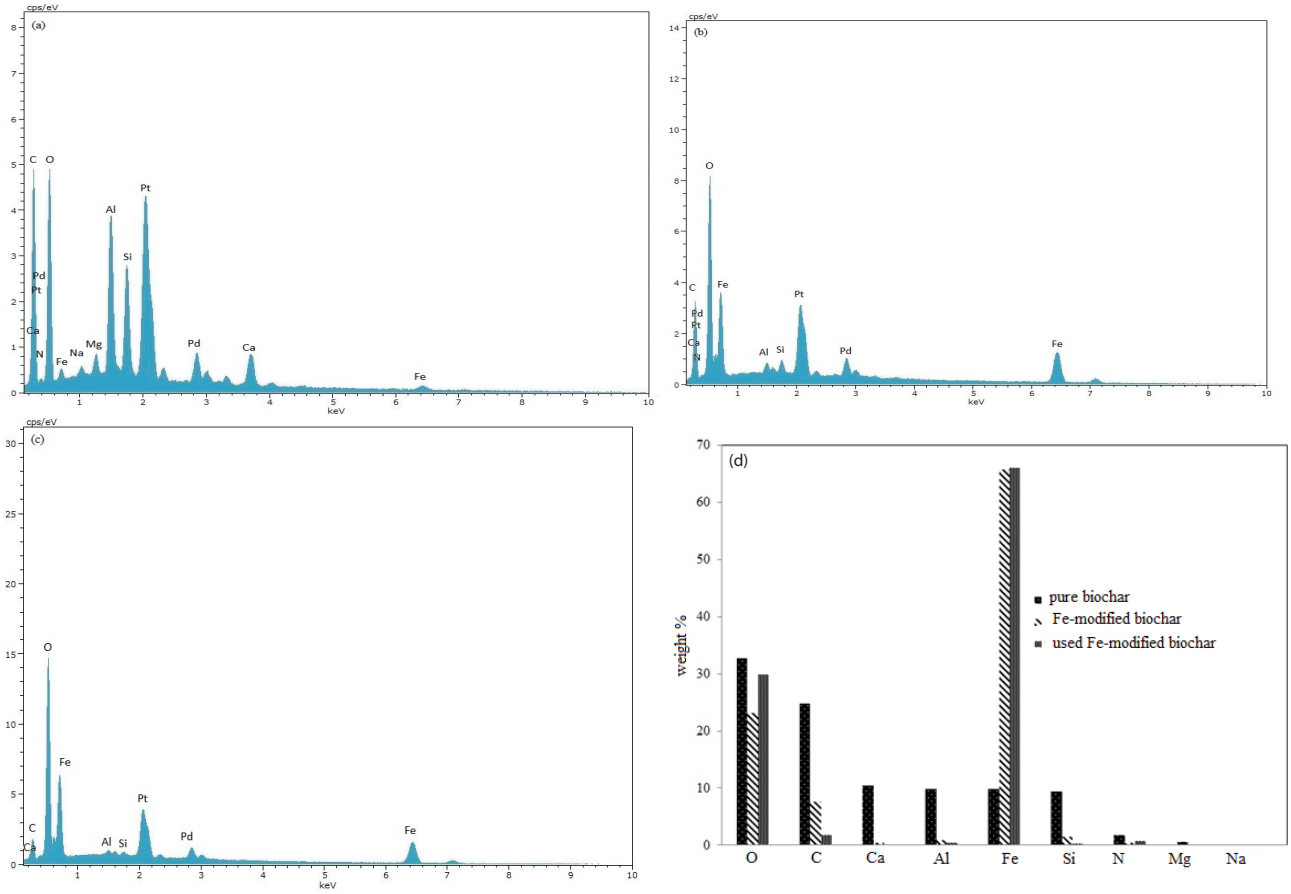

Fig. 2. EDX analysis of: (a) original biochar, (b) Fe-modified biochar c) MG-loaded Fe-modified biochar and (d) weight percentage of elements.

surface area can exceed 100 m^2/g [46]. Therefore, Fe modification of biochar can either increase or decrease its surface area, depending on the initial surface area of the precursor and the particle size of magnetite on the biochar surface [47,48]. In our case, the total pore volume as well as the average pore diameter were also increased after Fe modification (from 0.034 to 0.22 mL/g and 3.64 to 10.23 nm, respectively). The increase in total pore volume is consistent with the increase in surface area. The enlargement of the average pore diameter combined with the reduction of micropore area and volume lead to the conclusion that Fe-modified biochar lost almost all of the microporous structure and became essentially mesoporous. Table 4 presents the pore size distribution and the corresponding pore volumes and areas of Fe-modified biochar, where it can be seen that mesopores determine to a large extent the total pore volume and area. It is possible that Fe_3O_4 particles crushed into the biochar surface and created more pores and enlarged previous ones [43].

According to the IUPAC classification of physisorption isotherms, both biochars show a combination of type II and IV(a) adsorption isotherms (Figs. 4(a) and (b)) [49]. Both isotherms are practically the same until p/p_o = 0.8; however, the adsorption isotherm for the original biochar resembled more of a type II isotherm after that point, whereas the Fe-modified biochar isotherm essentially became type IV(a). Type II isotherm is the result of unrestricted monolayer–multilayer adsorption up to high p/p_o. A more gradual curvature at the lower p/p_o end is an indication of a significant amount of overlap of monolayer coverage and the onset of multilayer adsorption. Type IV isotherms are typically given by mesoporous adsorbents. The adsorption behavior in mesopores is determined by the adsorbent–adsorptive interactions and also by the interactions between the molecules in the condensed state. In this case, the initial monolayer–multilayer adsorption on the mesopore walls, which takes the same path as the corresponding part of a type II isotherm, is followed by pore condensation [49]. The original biochar isotherm corresponds to H3 hysteresis loop, whereas the one of Fe-modified biochar to H2(b). Type H3 hysteresis is usually found on solids with a very wide distribution of pore size. Type H2 corresponds to channels with a pore mouth smaller than the pore body (this is the case of ink-bottle-shaped pores).

3.2. MG adsorption

The actual experimental as well as the percentage adsorption values predicted by the box-behnken design are shown in Table 2. These results were used to calculate the coefficients of the quadratic (second-order) polynomial regression equation which expressed the empirical relationship between the response and independent variables (Eq. (5)).

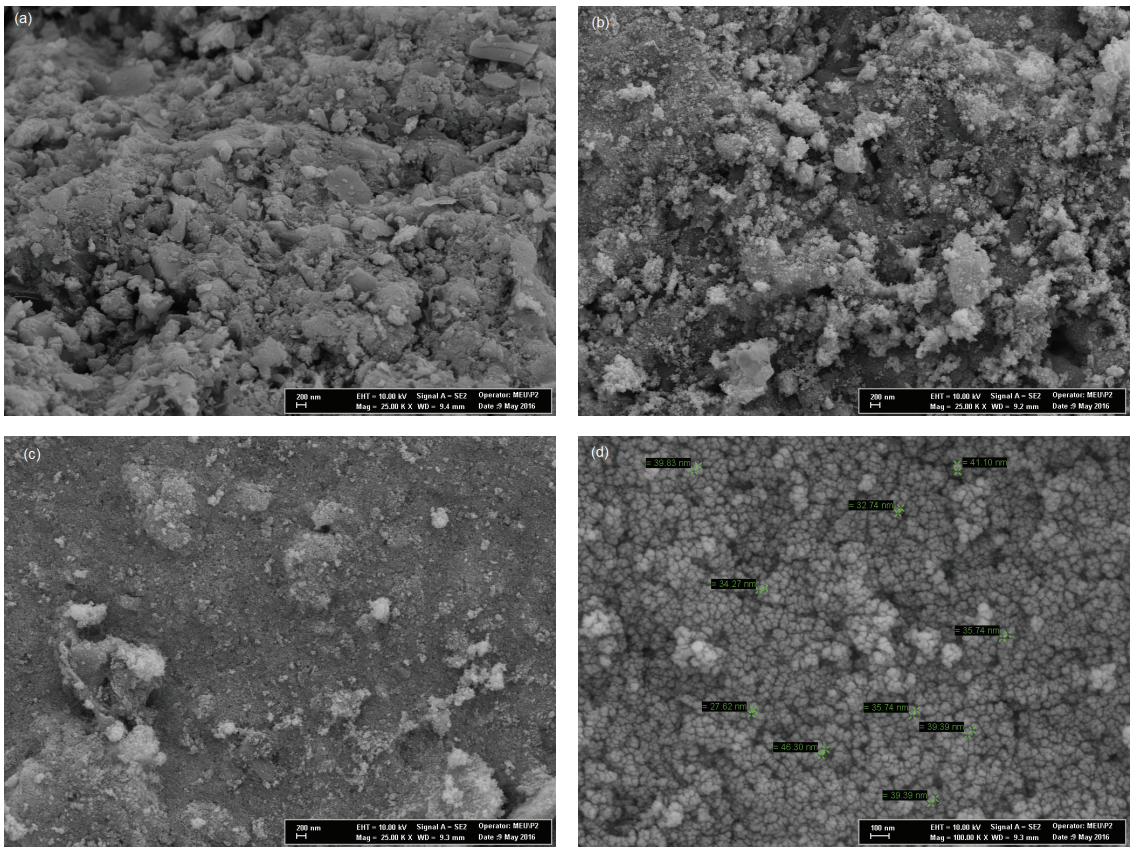

Fig. 3. Scanning electron microscopy images of: (a) original biochar, (b) Fe-modified biochar, (c) and (d) MG-loaded Fe-modified biochar (200 and 100 nm, respectively).

Table 3
Surface area characterization of original biochar and Fe-modified biochar

	Original biochar	Fe-modified biochar
Surface area (m^2/g)	38.1	89
Total pore volume (mL/g)	0.034	0.22
Average pore diameter (nm)	3.64	10.23
Micropore area (m^2/g)	10.66 (27.9% of total)	4.08 (4.58% of total)
Micropore volume (mL/g)	0.0051 (15% of total)	0.0012 (0.54% of total)

$$\text{Adsorption } \% = +96.38 - 1.81X_{C_0} + 1.73X_{pH} + 1.20X_t + 3.33X_T - 2.44X_{Co}^2 - 12.26X_{pH}^2 - 3.08X_t^2 - 3.49X_T^2 \quad (5)$$

At each and all conditions, there is a high level of agreement between the experimental adsorption percentage and the predicted values. In order to ensure the statistical significance of the quadratic model employed for fitting the experimental data at a 95% confidence level, the model was tested by ANOVA. The impact and significance of each term of Eq. (5) and the results are presented in Table 5. The model *F* value of 189.50 implies that the model proposed is significant and

Table 4
Pore size distribution of Fe-modified biochar

	Pore width range (nm)	Pore volume (cm^3)	Pore area (m^2/g)
Mesopores	18.27 – 12.54	0.0522	14.61
	12.54 – 9.6	0.0285	10.74
	9.6 – 7.68	0.0181	8.66
	7.68 – 6.42	0.0119	6.91
	6.42 – 5.52	0.0086	5.88
	5.52 – 4.78	0.0066	5.23
	4.78 – 4.2	0.0056	5.07
	4.2 – 3.73	0.0046	4.65
	3.73 – 3.33	0.0039	4.54
	3.33 – 2.98	0.0035	4.49
	2.98 – 2.67	0.0031	4.51
	2.67 – 2.39	0.0029	4.66
	2.39 – 2.14	0.0028	4.99
Micropores	2.14 – 1.89	0.0026	5.30
	1.89 – 1.65	0.0026	5.96

there is only a 0.01% chance that an F value of this order could occur due to noise. The lack-of-fit F value is 2.72 confirming that it is not significantly relative to pure error. The terms that were not addressed by the ANOVA were the non-significant terms ($p > 0.05$) and they were removed from the initial model. The correlation coefficients indicate the reliability of the quadratic model. The obtained R^2 and R^2_{adj} values were 0.9870 and 0.9819, respectively. This implies that 98.70% of the variations for MG adsorption percentage are explained by the independent variables. In addition, the robustness of the model is shown by comparing the experimental vs. predicted values (Fig. 5). It is clear that the predicted values are very close to the actual experimental ones, thus confirming the stability of the regression model proposed. The optimum experimental adsorption percentage of 97.16% was obtained at a pH value of 6, initial MG concentration of 7.5 ppm, temperature of 30°C and treatment time of 20 min.

Using Eq. (5) and setting 90% as the minimum acceptable MG adsorption, the process was optimized within the parameter limits described in section 2.4. Within these boundaries, the theoretical optimum conditions were predicted as: initial MG concentration 6.56 ppm, temperature 34.75°C, adsorption time 22 min and pH 6.14, where 98% adsorption could be achieved. For comparison reasons, MG adsorption was tested on the original biochar sample at the optimum conditions described above. An adsorption of 63.5% was obtained, which is considerably lower than the corresponding value from the Fe-modified biochar. This difference is probably

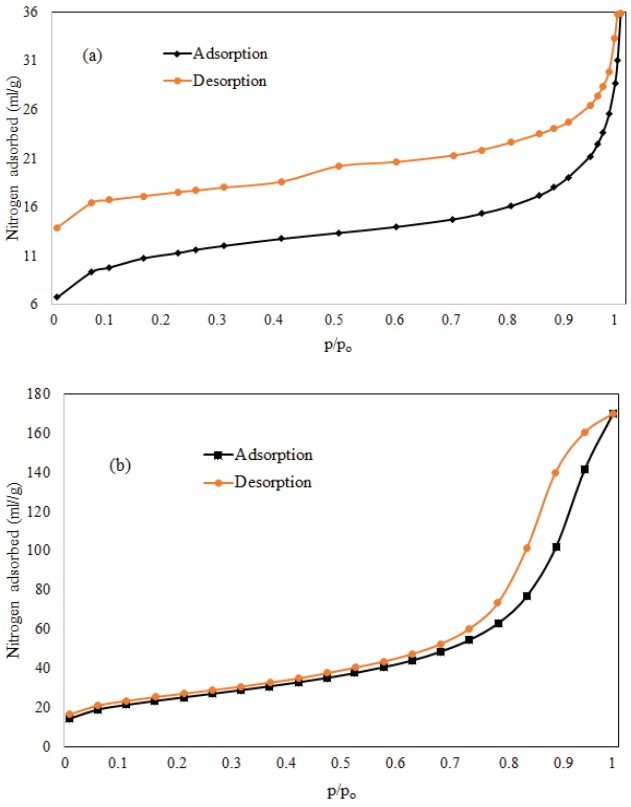

Fig. 4. Nitrogen adsorption/desorption isotherms for: (a) original biochar and (b) Fe-modified biochar.

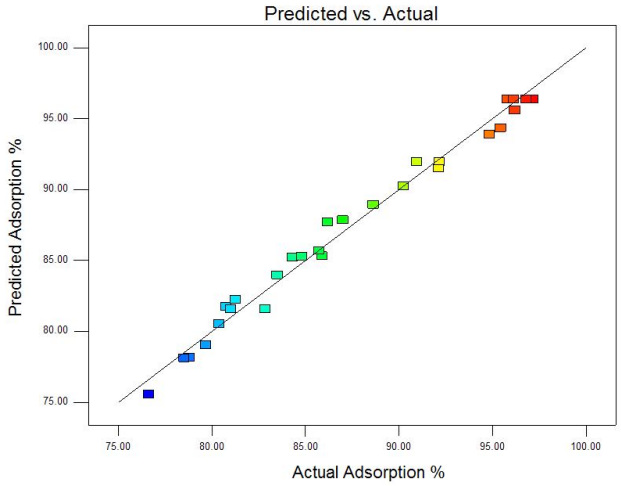

Fig. 5. Actual vs. predicted values for adsorption percentage of MG.

Table 5
ANOVA results of the quadratic model for MG removal by Fe-modified biochar

Source	Sum of square	Degrees of freedom	Mean square	F value	p Value
Model	1,211.90	8	151.49	189.50	<0.0001
X_{Co}	39.35	1	39.35	49.22	<0.0001
X_{pH}	35.81	1	35.81	44.80	<0.0001
X_t	17.14	1	17.14	21.44	0.0002
X_T	133.07	1	133.07	166.45	<0.0001
X_{Co}^2	38.53	1	38.53	48.20	<0.0001
X_{pH}^2	974.94	1	974.94	1,219.56	<0.0001
X_t^2	61.38	1	61.38	76.78	<0.0001
X_T^2	78.94	1	78.94	98.75	<0.0001
Residual	15.99	20	0.80		
Lack-of-fit	14.64	16	0.92	2.72	0.1722
Pure error	1.35	4	0.34		
Corrected total	1,227.89	28			

due to the higher surface area as well as the introduction of chemical moieties on the surface of the Fe-modified sample, as described earlier in section 3.1. Therefore, in our case the impregnation of biochar with magnetite particles not only promoted easier recovery after treatment, but also increased the adsorption capacity of the adsorbent.

3.3. Significance and interactive effects of the independent variables

The percentage adsorption of MG on the biochar surface was positively dependent on temperature ($p < 0.0001$), time ($p = 0.0002$) and pH ($p < 0.0001$), with temperature being the single most significant parameter at linear level due to the highest regression coefficient of 3.33 (Eq. (5)). The initial dye concentration showed negative influence on the adsorption efficiency with a –1.81 coefficient value. All quadratic terms showed significant effects, with pH having the highest coefficient (–12.26).

3.3.1. Three-dimensional response surfaces

Based on the model equation (Eq. (5)), the response surface plots of the variables (surface and contour plots) were

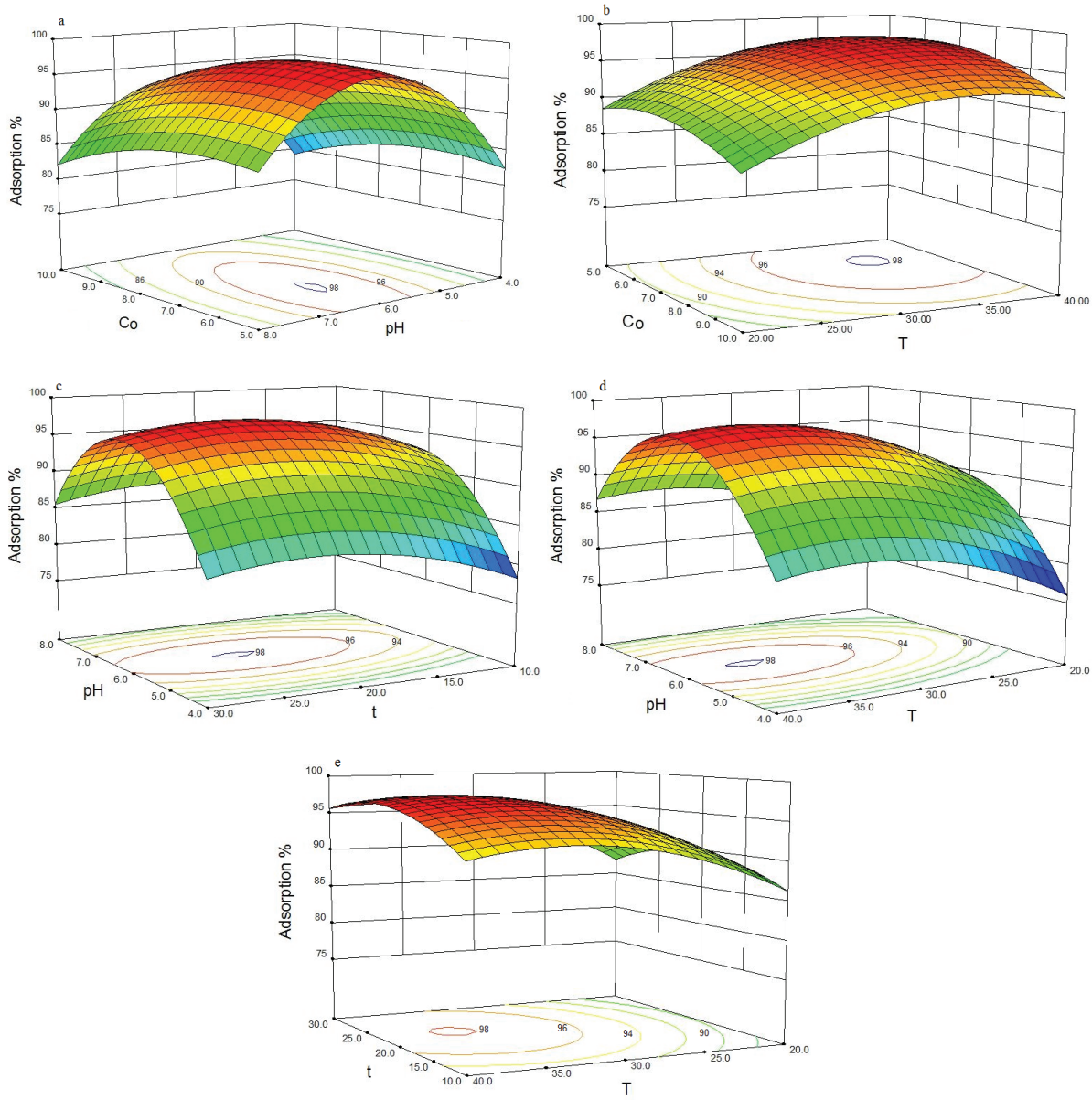

Fig. 6. Response surface plots showing the effects of temperature, pH, time and initial MG concentration on MG adsorption: (a) initial dye concentration against pH at fixed optimal time of 22 min and temperature of 34.75°C, (b) initial dye concentration against temperature at fixed optimal time and pH of 6.14, (c) pH against time at fixed optimal temperature and initial concentration of 6.56 ppm, (d) pH against temperature at fixed optimum time and initial dye concentration and (e) time against temperature at fixed optimum pH and initial dye concentration.

drawn. Fig. 6(a) shows the combined effect of the initial MG concentration and pH on MG adsorption (at the optimum temperature of 34.75°C and treatment time 22 min). At any given pH between 4 and 8, lowering the initial MG concentration only marginally improved the adsorption percentage. For example, at pH 4 adsorption only increased from 78% to 83% when C_0 was decreased from 10 to 5 ppm. This indicated that there was no significant competition of MG molecules for sorption sites on the sorbent surface area at this concentration range. On the other hand, as in many adsorption processes the role of pH was dominant. The most effective adsorption was observed in the pH range of 5.5–6.5 and the optimum pH value was determined to be 6.16 (95% MG adsorption). At either end of the experimental pH range, adsorption percentage was reduced considerably. MG gives positively charged ions when dissolved in water, therefore, at lower pH values it competes with hydrogen ions for adsorption onto the adsorbent surface leading to a decrease in the amount of MG adsorbed. If protons are attached to the adsorbent surface, repulsive forces will be generated between MG molecules and adsorbent surface. The high adsorption capacity of MG at near-neutral pH values on Fe-modified biochar may be explained due to the electrostatic attraction that occurred between adsorbent surfaces and MG. These conclusions largely agree with the findings of Dastkhoon et al. [50] who optimized MG adsorption on zinc sulfide:copper nanoparticle-loaded on activated carbon. They achieved an optimum 97.86% adsorption at a pH value of 6 and their experimental values were in good agreement with the predicted ones. Similarly, Zheng et al. [51] achieved an optimum MG adsorption of 96.49% at the same pH value using magnetic litchi pericarp as adsorbent.

The pH_{pzc} value was determined as 6.8 and provided an important insight on the surface chemistry of the process (Fig. 7). At pH values below pH_{pzc} the adsorbent's surface acquired an overall positive charge that accounted for the low attraction—and therefore low removal—of MG. As the pH of solution gradually increased and exceeded the pH_{pzc} value, the adsorbent's surface became negatively charged and the cationic MG molecules were increasingly attracted leading to higher removal percentage.

Fig. 6(b) presents the combined effect of initial MG concentration and temperature on MG adsorption (pH and time constant at the optimum values). Adsorption experiments were carried in the temperature range of 20°C–40°C. The temperature effect on the adsorption efficiency was observed positive up to 34.75°C which is determined as the optimum temperature, but then it showed a slight downward trend. The increase in temperature accelerates the diffusion rate of dye molecules into the pores of the adsorbent, indicating that the adsorption process is probably endothermic. Additionally, the viscosity of the medium decreased as the temperature was raised thus facilitating the formation of cavitation bubbles due to the propagation of the ultrasonic sound waves [52]. Ultrasonic waves play an active role in the formation of new active sites, enhance the mass and heat transfer rate on and at the adsorbent surface [53,54]. Beyond the optimum temperature of 34.75°C, it appears that thermal desorption of MG competed with adsorption.

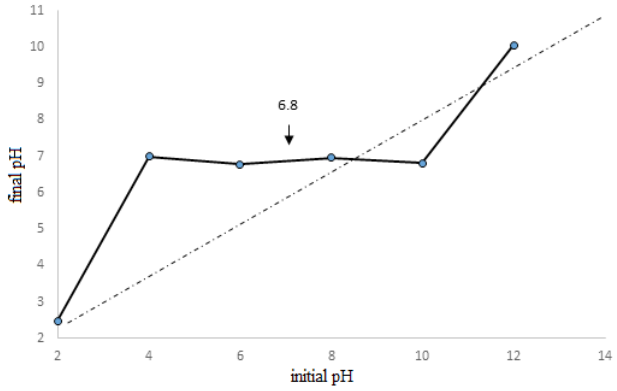

Fig. 7. Plot for the determination of pH_{pzc}.

Fig. 6(c) shows the combined effect of pH and time on MG adsorption (temperature and initial MG concentration constant at the optimum values). As shown earlier in Fig. 6(a), pH plays a very important role in the process. Time had a much lesser effect and at any given pH, MG adsorption percentage increased ~5% as time increased from 10 to 25 min. This may be due to the promotion of MG molecules dispersion in solution via ultrasonic power [55]. However, the lengthening of sonication time can cause the weakly adsorbed dye molecules to escape from the pores. An almost identical trend was observed in Fig. 6(d), where the interactive effect of pH and temperature can be observed. A twofold raise in temperature resulted in ~10% increase in MG adsorption.

Fig. 6(e) presents the interactive effect between time and temperature at a pH value of 6.16 and initial MG concentration of 6.56 ppm. The effect of temperature was more obvious at longer adsorption times (>25 min), where increasing the temperature generally increased MG adsorption more than 8%. At lower times, the corresponding increase was ~5%. As in Fig. 5(c), time in this case did not affect MG adsorption percentage significantly, confirming the optimum time determined earlier at 22 min.

3.4. Adsorption equilibrium isotherms

The MG and Fe-modified biochar relationship at equilibrium was further studied by fitting the experimental data on the Langmuir and Freundlich isotherm models. The theoretical background and corresponding equations of these models have been described in detail elsewhere [32,50,56]. Briefly, the Langmuir isotherm assumes monolayer adsorption onto a surface containing a specific number of adsorption sites, whereas the Freundlich isotherm is an empirical model that describes adsorption on the basis that surface consist of adsorption sites of varying affinities (heterogeneous). The isotherm constants and the correlation coefficients with the experimental data are listed in Table 6. The Langmuir isotherm provided a slightly better fit than the Freundlich isotherm (correlation coefficient 0.960 and 0.949, respectively). The maximum adsorption capacity (q_{max}) of 172.4 mg/g compares favorably with those capacities of modified or unmodified natural adsorbents. $1/n$ is a dimensionless parameter reflecting heterogeneity. The $1/n$ value of 0.75 indicates favorable adsorption. The n value of 1.32 is lower compared with many other adsorbents of Table 6, indicating higher degree of homogeneity [32].

Table 6
Comparison of isotherm parameters obtained in this work to other MG adsorption studies

Langmuir parameters			Freundlich parameters			Adsorbent used	Citation
q_{max} (mg/g)	b (L/mg)	R^2	K_f	n	R^2		
172.413	0.168	0.960	19.05	1.32	0.949	Fe-modified biochar	This work
168.067	9.44	0.999	8.298	6.13	0.936	ZnS/Cu nanoparticles on activated carbon	[50]
127.3	0.417	nr[a]	nr	nr	nr	Magnetic biochar	[56]
70.42	0.23	0.98	21.32	3.49	0.86	Magnetic litchi pericarps	[51]
87.72	0.575	0.998	4.367	1.54	0.987	CuO nanoparticles on activated carbon	[9]
101.215	3.283	0.999	6.396	2.21	0.939	Mn-doped Fe_3O_4 nanoparticle loaded activated carbon	[10]
202.429	10.978	0.997	10.256	2.65	0.920	Mn-doped ZnS nanoparticles on activated carbon	[8]
207.04	0.591	0.997	6.49	2.52	0.962	Fe_2O_3 nanoparticles on activated carbon	[11]
542	nr	nr	nr	nr	nr	Magnetite nanoparticles on mesoporous silica	[13]
909	0.050	0.996	159	0.32	0.907	Functionalized cross-linked poly(methyl acrylate)	[12]
35.84	0.039	0.731	0.335	1.05	0.998	*Cerastoderma lamarcki* shell	[16]
370	0.060	0.998	25.7	1.97	0.859	Cellulose modified with maleic anhydride	[57]
111	0.028	0.998	8.99	2.42	0.948	Cellulose modified with phthalic anhydride	[57]
131.9	0.483	0.999	43.69	3.1	0.915	Modified epoxy-cellulose	[58]
458.7	0.268	0.993	93.65	2.23	0.915	Cellulose-based multicarboxyl	[59]

[a]Not reported.

Table 7
Parameters of the pseudo-first-order, pseudo-second-order and intra-particle diffusion models

Kinetic model	Parameter	Value
Pseudo-first order	q_e, experimental (mg/g)	9.064
	q_e, calculated (mg/g)	2.185
	k_A (min^{-1})	0.0645
	R^2	0.9508
Pseudo-second order	q_e, experimental (mg/g)	9.064
	q_e, calculated (mg/g)	9.24
	k_B (g/mg/min)	0.046
	R^2	0.9818
Intra-particle diffusion	k_{int} ($mg/g/min^{1/2}$)	0.8143
	C (mg/g)	4.34
	R^2	0.9621

3.5. Adsorption kinetics

The dynamics of the adsorption were investigated in terms of the order of the rate constant. The rate-controlling mechanisms of the adsorption process are commonly studied by applying the pseudo-first-order (Lagergren's model), pseudo-second-order and intra-particle diffusion kinetic models. The theoretical details and corresponding models' equations can be found in previous works [32,51,56]. The properties and constants corresponding to each model are shown in Table 7. The pseudo-second-order correlation coefficient provided a better fit for the data (0.9818) compared with the pseudo-first-order and intra-particle coefficients (0.9508 and 0.9621). Additionally, the calculated q value closely matched the experimental value, indicating that the adsorption process followed the pseudo-second-order model and chemisorption is the rate-controlling process. This conclusion agrees well with the findings of other researchers who studied MG adsorption on other adsorbents [9,10,50,51,56]. The parameter C of the intra-particle diffusion model corresponds to the thickness of the boundary layer. If the value of C is zero, this means that adsorption is exclusively controlled by the intra-particle diffusion mechanism. However, a value of 4.34 indicates that boundary layer effects are not negligible and co-exist with chemisorption.

4. Conclusions

Either as a dye or antifungal drug, residual concentrations of MG pose a threat to the environment. Fe-modified biochar proved to be an effective adsorbent for MG under a wide range of conditions. At all conditions tested, the adsorption percentage ranged between 79% and 97%. In practice, the highest value of 97.16% was obtained at a pH value of 6, initial MG concentration of 7.5 ppm, temperature of 30°C and treatment time of 20 min. The use of RSM, predicted a theoretical maximum adsorption percentage of 98%, at pH 6.16, initial MG concentration of 6.56 ppm, temperature of 34.75°C and treatment time of 22 min. Compared with the original biochar, the Fe-modified sample improved the adsorption of MG by ~34%. Of all the parameters tested, pH was found to be the most influential. The adsorption process was best described by the Langmuir model and the maximum adsorption capacity of 172.3 mg/g compared favorably with other natural adsorbents. Kinetically, adsorption primarily followed the pseudo-second-order model, supplemented by boundary layer effects.

Acknowledgments

The authors would like to thank Sonnenerde GmbH and Hans-Peter Schmidt (Ithaka Institute, Ayent, Valais, Switzerland) for the biochar sample. This research did not receive any specific grant from funding agencies in the public, commercial or not-for-profit sectors.

References

[1] S. Srivastava, R. Sinha, D. Roy, Toxicological effects of malachite green, Aquat. Toxicol., 66 (2004) 319–329.
[2] A. Stammati, C. Nebbia, I. De Angelis, A.G. Albo, M. Carletti, C. Rebecchi, F. Zampaglioni, M. Dacasto, Effects of malachite green (MG) and its major metabolite, leucomalachite green (LMG), in two human cell lines, Toxicol. in Vitro, 19 (2005) 853–858.
[3] The Commison of the European Communities, Commission Decision (2003/181/EC) of 13 March 2003 amending Decision 2002/657/EC as regards the setting of minimum required performance limits (MRPLs) for certain residues in food of animal origin, Off. J. Eur. Union, L71 (2003) 17–18.
[4] R.M. Mohamed, D. McKinney, M.W. Kadi, I.A. Mkhalid, W. Sigmund, Platinum/zinc oxide nanoparticles: enhanced photocatalysts degrade malachite green dye under visible light conditions, Ceram. Int., 42 (2016) 9375–9381.
[5] C.G. Liu, T. Zheng, S. Liu, H.Y. Zhang, Photodegradation of malachite green dye catalyzed by Keggin-type polyoxometalates under visible-light irradiation: transition metal substituted effects, J. Mol. Struct., 1110 (2016) 44–52.
[6] D. Pathania, R. Katwal, G. Sharma, M. Naushad, M.R. Khan, A.H. Al-Muhtaseb, Novel guar gum/Al_2O_3 nanocomposite as an effective photocatalyst for the degradation of malachite green dye, Int. J. Biol. Macromol., 87 (2016) 366–374.
[7] M.W. Kadi, D. McKinney, R.M. Mohamed, I.A. Mkhalid, W. Sigmund, Fluorine doped zinc oxide nanowires: enhanced photocatalysts degrade malachite green dye under visible light conditions, Ceram. Int., 42 (2016) 4672–4678.
[8] A. Asfaram, M. Ghaedi, F. Yousefi, M. Dastkhoon, Experimental design and modeling of ultrasound assisted simultaneous adsorption of cationic dyes onto ZnS: Mn-NPs-AC from binary mixture, Ultrason. Sonochem., 33 (2016) 77–89.
[9] E.A. Dil, M. Ghaedi, A. Asfaram, S. Hajati, F. Mehrabi, A. Goudarzi, Preparation of nanomaterials for the ultrasound-enhanced removal of Pb^{2+} ions and malachite green dye: chemometric optimization and modeling, Ultrason. Sonochem., 34 (2017) 677–691.
[10] A. Asfaram, M. Ghaedi, S. Hajati, A. Goudarzi, E.A. Dil, Screening and optimization of highly effective ultrasound-assisted simultaneous adsorption of cationic dyes onto Mn-doped Fe_3O_4-nanoparticle-loaded activated carbon, Ultrason. Sonochem., 34 (2017) 1–12.
[11] A. Asfaram, M. Ghaedi, S. Hajati, A. Goudarzi, Synthesis of magnetic γ-Fe_2O_3-based nanomaterial for ultrasonic assisted dyes adsorption: modeling and optimization, Ultrason. Sonochem., 32 (2016) 418–431.
[12] A. Pourjavadi, A. Abedin-Moghanaki, Ultrafast and efficient removal of cationic dyes using a magnetic nanocomposite based on functionalized cross-linked poly(methylacrylate), React. Funct. Polym., 105 (2016) 95–102.
[13] M. Brigante, E. Pecini, M. Avena, Magnetic mesoporous silica for water remediation: synthesis, characterization and application as adsorbent of molecules and ions of environmental concern, Microporous Mesoporous Mater., 230 (2016) 1–10.
[14] X. Li, Y. Zhang, L. Jing, X. He, Novel N-doped CNTs stabilized Cu_2O nanoparticles as adsorbent for enhancing removal of Malachite Green and tetrabromobisphenol A, Chem. Eng. J., 292 (2016) 326–339.
[15] B. Nanda, A.C. Pradhan, K.M. Parida, A comparative study on adsorption and photocatalytic dye degradation under visible light irradiation by mesoporous MnO_2 modified MCM-41 nanocomposite, Microporous Mesoporous Mater., 226 (2016) 229–242.
[16] S.Y. Kazemi, P. Biparva, E. Ashtiani, *Cerastoderma lamarcki* shell as a natural, low cost and new adsorbent to removal of dye pollutant from aqueous solutions: equilibrium and kinetic studies, Ecol. Eng., 88 (2016) 82–89.
[17] O. García-Rodríguez, J.A. Bañuelos, A. El-Ghenymy, L.A. Godínez, E. Brillas, F.J. Rodríguez-Valadez, Use of a carbon felt–iron oxide air-diffusion cathode for the mineralization of Malachite Green dye by heterogeneous electro-Fenton and UVA photoelectro-Fenton processes, J. Electroanal. Chem., 767 (2016) 40–48.
[18] H. Sun, W. Huang, H. Yang, S. Zhang, Co-immobilization of laccase and mediator through a self-initiated one-pot process for enhanced conversion of malachite green, J. Colloid Interface Sci., 471 (2016) 20–28.
[19] A.H. Lone, G.R. Najar, M.A. Ganie, J.A. Sofi, T. Ali, Biochar for sustainable soil health: a review of prospects and concerns, Pedosphere, 25 (2015) 639–653.
[20] T. Głąb, J. Palmowska, T. Zaleski, K. Gondek, Effect of biochar application on soil hydrological properties and physical quality of sandy soil, Geoderma, 281 (2016) 11–20.
[21] V. Pandey, A. Patel, D.D. Patra, Biochar ameliorates crop productivity, soil fertility, essential oil yield and aroma profiling in basil (*Ocimum basilicum* L.), Ecol. Eng., 90 (2016) 361–366.
[22] A.U. Rajapaksha, S.S. Chen, D.C.W. Tsang, M. Zhang, M. Vithanage, S. Mandal, B. Gao, N.S. Bolan, Y.S. Ok, Engineered/designer biochar for contaminant removal/immobilization from soil and water: potential and implication of biochar modification, Chemosphere, 148 (2016) 276–291.
[23] H.M. Anawar, F. Akter, Z.M. Solaiman, V. Strezov, Biochar: an emerging panacea for remediation of soil contaminants from mining, industry and sewage wastes, Pedosphere, 25 (2015) 654–665.
[24] A. Mahar, P. Wang, R. Li, Z. Zhang, Immobilization of lead and cadmium in contaminated soil using amendments: a review, Pedosphere, 25 (2015) 555–568.
[25] E. Agrafioti, D. Kalderis, E. Diamadopoulos, Ca and Fe modified biochars as adsorbents of arsenic and chromium in aqueous solutions, J. Environ. Manage., 146 (2014) 444–450.
[26] J. Hou, L. Huang, Z. Yang, Adsorption of ammonium on biochar prepared from giant reed, Environ. Sci. Pollut. Res., 23 (2016) 19107–19115. DOI: 10.1007/s11356–016–7084–4.
[27] K.K. Shimabuku, J.P. Kearns, J.E. Martinez, R.B. Mahoney, L. Moreno-Vasquez, R.S. Summers, Biochar sorbents for sulfamethoxazole removal from surface water, stormwater, and wastewater effluent, Water Res., 96 (2016) 236–245.
[28] M. Taheran, M. Naghdi, S.K. Brar, E.J. Knystautas, M. Verma, A.A. Ramirez, R.Y. Surampalli, J.R. Valero, Adsorption study of environmentally relevant concentrations of chlortetracycline on pinewood biochar, Sci. Total Environ., 571 (2016) 772–777.
[29] P. Nautiyal, K.A. Subramanian, M.G. Dastidar, Adsorptive removal of dye using biochar derived from residual algae after in-situ transesterification: alternate use of waste of biodiesel industry, J. Environ. Manage., 182 (2016) 187–197.
[30] M.E. Mahmoud, G.M. Nabil, N.M. El-Mallah, H.I. Bassiouny, S. Kumar, T.M. Abdel-Fattah, Kinetics, isotherm, and thermodynamic studies of the adsorption of reactive red 195 A dye from water by modified Switchgrass Biochar adsorbent, J. Ind. Eng. Chem., 37 (2015) 156–167.
[31] M. Saif Ur Rehman, I. Kim, N. Rashid, M. Adeel Umer, M. Sajid, J.I. Han, Adsorption of brilliant green dye on biochar prepared from lignocellulosic bioethanol plant waste, Clean Soil Air Water, 44 (2016) 55–62.
[32] M. Şener, B. Kayan, S. Akay, B. Gözmen, D. Kalderis, Fe-modified sporopollenin as a composite biosorbent for the removal of Pb^{2+} from aqueous solutions, Desal. Wat. Treat., 3994 (2016) 1–19.
[33] H.J. Bachmann, T.D. Bucheli, A. Dieguez-Alonso, D. Fabbri, H. Knicker, H.-P. Schmidt, A. Ulbricht, R. Becker, A. Buscaroli, D. Buerge, A. Cross, D. Dickinson, A. Enders, V.I. Esteves M.W.H. Evangelou, G. Fellet, K. Friedrich, G. Gasco-Guerrero, B. Glasier, U.M. Hanke, K. Hanley, I. Hilber, D. Kalderis, J. Leifeld, O. Masek, J. Mumme, M.P. Carmona, R.C. Pereira, F. Rees, A.G. Rombola`, J.M. de la Rosa, R. Sakrabani, S. Sohi, G. Soja, M. Valagussa, F. Verheijen, F. Zehetnery, Toward the standardization of biochar analysis: the COST Action TD1107 interlaboratory comparison, J. Agric. Food Chem., 64 (2016) 513–527.

[34] M.A. Kamboh, M. Yilmaz, Synthesis of *N*-methylglucamine functionalized calix[4]arene based magnetic sporopollenin for the removal of boron from aqueous environment, Desalination, 310 (2013) 67–74.
[35] G. Newcombe, R. Hayes, M. Drikas, Granular activated carbon: Importance of surface properties in the adsorption of naturally occurring organics, Colloids Surf., A, 78 (1993) 65–71.
[36] A.R. Bagheri, M. Ghaedi, A. Asfaram, A.A. Bazrafshan, R. Jannesar, Comparative study on ultrasonic assisted adsorption of dyes from single system onto Fe_3O_4 magnetite nanoparticles loaded on activated carbon: experimental design methodology, Ultrason. Sonochem., 34 (2017) 294–304.
[37] M.A. Bezerra, R.E. Santelli, E.P. Oliveira, L.S. Villar, L.A. Escaleira, Response surface methodology (RSM) as a tool for optimization in analytical chemistry, Talanta, 76 (2008) 965–977.
[38] S.S. Mayakaduwa, P. Kumarathilaka, I. Herath, M. Ahmad, M. Al-Wabel, Y.S. Ok, A. Usman, A. Abduljabbar, M. Vithanage, Equilibrium and kinetic mechanisms of woody biochar on aqueous glyphosate removal, Chemosphere, 144 (2016) 2516–2521.
[39] S. Fan, J. Tang, Y. Wang, H. Li, H. Zhang, J. Tang, Z. Wang, X. Li, Biochar prepared from co-pyrolysis of municipal sewage sludge and tea waste for the adsorption of methylene blue from aqueous solutions: kinetics, isotherm, thermodynamic and mechanism, J. Mol. Liq., 220 (2016) 432–441.
[40] X. Guo, H. Dong, C. Yang, Q. Zhang, C. Liao, F. Zha, L. Gao, Application of goethite modified biochar for tylosin removal from aqueous solution, Colloids Surf., A, 502 (2016) 81–88.
[41] J.T. Mayo, C. Yavuz, S. Yean, L. Cong, H. Shipley, W. Yu, J. Falkner, A. Kan, M. Tomson, V.L. Colvin, The effect of nanocrystalline magnetite size on arsenic removal, Sci. Technol. Adv. Mater., 8 (2007) 71–75.
[42] V. Sureshkumar, S.C.G. Kiruba Daniel, K. Ruckmani, M. Sivakumar, Fabrication of chitosan–magnetite nanocomposite strip for chromium removal, Appl. Nanosci., 6 (2015) 277–285.
[43] D. Shan, S. Deng, T. Zhao, B. Wang, Y. Wang, J. Huang, G. Yu, J. Winglee , M.R. Wiesner, Preparation of ultrafine magnetic biochar and activated carbon for pharmaceutical adsorption and subsequent degradation by ball milling, J. Hazard. Mater., 305 (2016) 156–163.
[44] B. Chen, Z. Chen, S. Lv, A novel magnetic biochar efficiently sorbs organic pollutants and phosphate, Bioresour. Technol., 102 (2011) 716–723.
[45] Q. Song, B. Yang, H. Wang, S. Xu, Y. Cao, Effective removal of copper (II) and cadmium (II) by adsorbent prepared from chitosan-modified magnetic biochar, J. Residuals Sci. Technol., 13 (2016) 197–205.
[46] R.M. Cornell, U. Schwertmann, The Iron Oxides, VCH Press, Weinheim, Germany, 1996.
[47] L. Trakal, V. Veselská, I. Šafařík, M. Vítková, S. Číhalová, M. Komárek, Lead and cadmium sorption mechanisms on magnetically modified biochars, Bioresour. Technol., 203 (2016) 318–324.
[48] Y. Han, X. Cao, X. Ouyang, S.P. Sohi, J. Chen, Adsorption kinetics of magnetic biochar derived from peanut hull on removal of Cr(VI) from aqueous solution: effects of production conditions and particle size, Chemosphere, 145 (2016) 336–341.
[49] M. Thommes, K. Kaneko, A.V. Neimark, J.P. Olivier, F. Rodriguez-Reinoso, J. Rouquerol, K.S.W. Sing, Physisorption of gases, with special reference to the evaluation of surface area and pore size distribution (IUPAC Technical Report), Pure Appl. Chem., 87 (2015) 1051–1069.
[50] M. Dastkhoon, M. Ghaedi, A. Asfaram, A. Goudarzi, S.M. Langroodi, I. Tyagi, S. Agarwal, V.K. Gupta, Ultrasound assisted adsorption of malachite green dye onto ZnS:Cu-NP-AC: equilibrium isotherms and kinetic studies – response surface optimization, Sep. Purif. Technol., 156 (2015) 780–788.
[51] H. Zheng, J. Qi, R. Jiang, Y. Gao, X. Li, Adsorption of malachite green by magnetic litchi pericarps: a response surface methodology investigation, J. Environ. Manage., 162 (2015) 232–239.
[52] A. Hassani, R. Darvishi Cheshmeh Soltani, M. Kıranşan, S. Karaca, C. Karaca, A. Khataee, Ultrasound-assisted adsorption of textile dyes using modified nanoclay: central composite design optimization, Korean J. Chem. Eng., 32 (2015) 1–11.
[53] E. Şayan, Optimization and modeling of decolorization and COD reduction of reactive dye solutions by ultrasound-assisted adsorption, Chem. Eng. J., 119 (2006) 175–181.
[54] M. Roosta, M. Ghaedi, N. Shokri, A. Daneshfar, R. Sahraei, A. Asghari, Optimization of the combined ultrasonic assisted/adsorption method for the removal of malachite green by gold nanoparticles loaded on activated carbon: experimental design, Spectrochim. Acta, Part A, 118 (2014) 55–65.
[55] M. Jamshidi, M. Ghaedi, K. Dashtian, A.M. Ghaedi, S. Hajati, A. Goudarzi, E. Alipanahpour, Highly efficient simultaneous ultrasonic assisted adsorption of brilliant green and eosin B onto ZnS nanoparticles loaded activated carbon: artificial neural network modeling and central composite design optimization, Spectrochim. Acta, Part A, 153 (2015) 257–267.
[56] I. Šafařik, Z. Maděrova, K. Pospišková, H.-P. Schmidt, E. Baldiková, J. Filip, M. Křížek, O. Malina, M. Šafaříková, Magnetically modified biochar for organic xenobiotics removal, Water Sci. Technol., 74 (2016) 1706–1715.
[57] Y. Zhou, Y. Min, H. Qiao, Q. Huang, E. Wang, T. Ma, Improved removal of malachite green from aqueous solution using chemically modified cellulose by anhydride, Int. J. Biol. Macromol., 74 (2015) 271–277.
[58] Y. Zhou, X. Wang, M. Zhang, Q. Jin, B. Gao, T. Ma, Removal of Pb(II) and malachite green from aqueous solution by modified cellulose, Cellulose, 21 (2014) 2797–2809.
[59] Y. Zhou, M. Zhang, X. Hu, X. Wang, J. Niu, T. Ma, Adsorption of cationic dyes on a cellulose-based multicarboxyl adsorbent, J. Chem. Eng. Data, 58 (2013) 413–421.